Research Square

Preprints are preliminary reports that have not undergone peer review.
They should not be considered conclusive, used to inform clinical practice,
or referenced by the media as validated information.

Landscape configuration and peripheral network decoupling during stress recovery

Tian Gao

tian.gao@nwsuaf.edu.cn

College of Landscape Architecture and Arts, Northwest A&F University

Kejin Ma

College of Landscape Architecture and Arts, Northwest A&F University https://orcid.org/0009-0003-6696-2309

Mingyuan Gao

College of Landscape Architecture and Arts, Northwest A&F University

Yixin Zhang

College of Landscape Architecture and Arts, Northwest A&F University

Lifang Hu

College of Landscape Architecture and Arts, Northwest A&F University

Chengjin Lv

College of Landscape Architecture and Arts, Northwest A&F University

Ling Qiu

Article

Keywords: Landscape structure, Hierarchical decoupling, Psychoneuroimmunological networks, Virtual reality paradigm, Stress recovery kinetics

Posted Date: June 23rd, 2026

DOI: https://doi.org/10.21203/rs.3.rs-9896572/v1

License: This work is licensed under a Creative Commons Attribution 4.0 International License.
Read Full License

Additional Declarations: There is **NO** Competing Interest.

Abstract

Urban greening is widely promoted as a public health strategy, yet most evidence is still based on coarse vegetation metrics and cortico-centric accounts of restoration. Here, we tested whether landscape spatial configuration shapes stress recovery through peripheral rather than cortical pathways. In a full-factorial immersive virtual-reality stress paradigm, 157 adults were exposed to green and blue-green environments that varied in structural openness (10%, 50%, and 90%) after acute psychosocial stress. We continuously tracked cortical, autonomic, endocrine, and immune responses across stress and recovery phases. Acute stress produced a strongly peripheral-dominant perturbation, with large shifts in autonomic, endocrine, and immune markers but no detectable change in executive control network activity. During recovery, subjective responses converged across all natural settings relative to urban grey space, indicating a generalized affective benefit of natural exposure. In contrast, peripheral physiology remained highly configuration-sensitive. Sympathetic withdrawal dynamics and interleukin-6 (IL-6) suppression varied with the interaction between blue-green composition and structural openness, whereas parasympathetic rebound showed no spatial differentiation within the 30-min window. Executive control network (ECN) activity remained insensitive to landscape variation and instead followed baseline-dependent convergence. At the systems level, recovery was accompanied by a shift from a more integrated stress network to a more segregated recovery network, and reductions in peripheral cross-system connectivity statistically mediated anxiety relief. Together, these findings support a hierarchical model of environmental recovery in which landscape configuration is more consistently associated with peripheral autonomic-immune reorganization than with direct cortical modulation.

1. Introduction

Urbanization is reshaping everyday human exposure to stress, while also redefining the role of urban nature as a potential public-health resource. A substantial body of research now links nature exposure with improved mental health, reduced stress, and broader health benefits, which has helped position green and blue infrastructure as a key component of healthier cities[1, 2]. However, much of this evidence still relies on aggregate exposure metrics, such as greenness quantity, area, or accessibility, and is therefore most informative about whether nature matters, rather than which spatial forms matter most or why they matter biologically. This limitation is increasingly important because recent work suggests that the relationship between urban nature and mental health is not simply monotonic, and that generalized “more is better” assumptions may obscure the design characteristics that actually govern restorative benefit[1].

This unresolved issue is partly conceptual and partly methodological. Conceptually, urban nature is not a uniform exposure but a structured spatial experience shaped by visibility, enclosure, prospect, vegetation density, and the presence or absence of water. Yet these design properties are often collapsed into broad land-cover or dose indicators, making it difficult to determine how specific spatial configurations influence restoration. Evidence from blue-space research suggests that water can alter preference,

affect, and perceived restorativeness beyond green exposure alone[3], while work on prospect-refuge indicates that openness and enclosure are unlikely to be universally beneficial, because their effects depend on how safety, exposure, and environmental legibility are jointly perceived[4]. From an architectural neuroscience perspective, this means that the health value of urban nature should be understood not only as an issue of quantity, but also as an issue of spatial organization and experiential structure[5].

A second limitation concerns mechanism. Research on restorative environments has been strongly shaped by two influential traditions: Stress Recovery Theory (SRT), which emphasizes rapid affective and physiological recovery in natural settings[6], and Attention Restoration Theory (ART), which emphasizes the replenishment of directed attention in environments rich in softly fascinating stimuli[7]. These frameworks remain foundational, but much of the recent empirical literature has operationalized restoration primarily through self-report or cortical indicators, especially prefrontal measures associated with attentional control. That emphasis risks missing an important feature of stress biology: acute stress is a multisystem process involving coordinated shifts across autonomic, endocrine, immune, and brain systems rather than a purely cortical event. Neurovisceral integration research has long argued that cognitive, affective, and cardiovascular regulation are functionally linked[8], and Social Safety Theory (SST) further frames stress as a biologically embedded response that propagates through peripheral inflammatory and neuroendocrine pathways[9]. Taken together, these perspectives raise a more general question that extends beyond landscape psychology: when environments support recovery, do they do so mainly by directly modulating cortical control systems, or by first reorganizing peripheral stress physiology and thereby permitting higher-order stabilization?

Answering that question has been difficult in real-world settings, where environmental exposures are inherently confounded by weather, noise, crowding, route variability, and the co-occurrence of multiple spatial features. It has also been difficult because many studies on green space and health remain observational, making mechanistic pathways hard to isolate and validate rigorously[10]. Immersive virtual reality (VR) offers an important way forward by combining ecological relevance with experimental control, enabling researchers to manipulate spatial properties while holding non-target features constant[11]. For this reason, controlled virtual environments are particularly useful for testing whether recovery depends on the overall presence of nature, on specific typological attributes such as water, or on the interaction between landscape type and structural openness.

Against this background, the present study used a full-factorial immersive virtual-reality stress paradigm to examine how landscape configuration shapes multisystem stress recovery. By integrating subjective reports (STAI, PANAS), autonomic dynamics (SCL, RMSSD), salivary endocrine (cortisol, sAA) and immune biomarkers (IL-6, sIgA), and prefrontal hemodynamic responses (ECN HbO), this study moves beyond the simple question of whether urban nature is beneficial and addresses a broader question of human stress regulation: whether environmentally supported recovery is more consistently associated with peripheral physiological reorganization than with direct cortical modulation (Fig. 1). This question is

important not only for landscape research, but also for understanding how designed environments interact with the autonomic-immune-brain stress system in contemporary cities. With the overarching aim of determining how landscape spatial configuration influences multisystem stress recovery, and of clarifying whether these restorative effects are more consistently associated with peripheral decoupling than with direct cortical differentiation, the objectives of this study were as follows:

- Subjective-physiological comparison: Compare subjective affective recovery and peripheral physiological recovery across urban grey, green, and blue-green environments to determine whether generalized psychological relief masks deeper physiological divergence across spatial configurations.
- Mechanistic pathway evaluation: Examine whether stress recovery is more consistently associated with peripheral autonomic-immune reorganization than with landscape-specific variation in executive control network activity.
- Configuration effect identification: Test whether structural openness exerts a uniform restorative effect or whether its influence depends on landscape typology, particularly the distinction between pure-green and blue-green settings.

2. Methods and Materials

2.1 Study design and analytical hierarchy

This study employed a randomized between-subject, time-locked immersive virtual-reality (VR) experiment to examine how landscape spatial configuration shapes multisystem stress recovery under controlled conditions. Participants first underwent acute psychosocial stress induction and were then exposed to one of seven recovery environments in VR: three blue-green spaces, three pure-green spaces, and one urban grey control. The experimental structure followed a 3 × 2 full-factorial design defined by structural openness (10%, 50%, and 90% canopy cover) and landscape typology (blue-green vs. pure green), with urban grey space (UG) serving as a nature-deprived reference condition (Fig. 2).

To improve inferential clarity, outcomes were organized a priori into three analytical tiers. Primary outcomes were selected to represent the major levels of the proposed recovery pathway: state anxiety (STAI-S) as the principal subjective endpoint, skin conductance level (SCL) as the principal sympathetic kinetic marker, interleukin-6 (IL-6) and secretory immunoglobulin A (sIgA) as the principal peripheral inflammatory and mucosal immune markers, and executive control network oxygenated hemoglobin (ECN HbO) as the primary cortical endpoint. Secondary outcomes included positive and negative affect (PANAS), salivary cortisol, salivary alpha-amylase (sAA), and RMSSD. Exploratory analyses included Gaussian graphical modeling, network modularity and participation metrics, mediation analysis, and subgroup visualization of ECN trajectories. This hierarchy was defined to distinguish confirmatory recovery analyses from mechanistic and exploratory network analyses and to reduce interpretive inflation in a multimodal design.

2.2 VR environments and experimental stimuli

2.2.1 VR apparatus and technical specifications

The virtual environments were presented via the PICO 4 Ultra head-mounted display (HMD). Immersive virtual reality has been extensively validated as a highly ecologically valid surrogate for *in vivo* environmental exposure in environmental psychology and psychophysiology[12]. The HMD features dual 2.56-inch displays with a combined resolution of 2160 × 2160 per eye (1200 PPI) and a 105° field of view (FOV). Spatial positioning was achieved through four integrated cameras enabling six-degree-of-freedom (6DoF) tracking with sub-centimeter spatial accuracy. To minimize rendering latency, the HMD was connected to a high-performance workstation (NVIDIA RTX 5080, AMD Ryzen 7 9850X3D) via SteamVR USB 3.0 tethered link using AVC encoding. The simulation was maintained at a native 90 Hz refresh rate to ensure visual fluidity.

2.2.2 Landscape matrix and spatial standardization

Seven independent virtual scenarios were constructed within a constant 100 m × 60 m domain representing a compact urban park or streetscape. The factorial design comprised three openness levels (10%, 50%, and 90% canopy cover) crossed with two landscape typologies (blue-green and pure green), plus one urban grey control (UG) (Fig. 2). To isolate configuration effects, terrain, path geometry, architectural elements, benches, lighting fixtures, and other non-botanical visual objects were spatially standardized across the six nature-based conditions. Within blue–green scenarios, water-body footprint and base terrain were held constant; within pure-green scenarios, the same terrain and pathway logic were retained while excluding water. The principal manipulated variables were therefore the quantity, density, and spatial arrangement of vegetation required to achieve target canopy cover. The specific configurations of the seven landscape spatial typologies are as follows: (1) Open Blue-Green Space (BG-O, canopy cover 10%): Functioning as an expansive waterfront meadow, this scenario integrated scattered ponds and small lakes of varying sizes into a vast lawn. The sparse vegetation provided maximal prospect and long-range visual depth, mimicking the sweeping, unobstructed vistas of a wetland park edge (Fig. 2a)[13]. (2) Semi-Open Blue-Green Space (BG-SO, canopy cover 50%): Analogous to a savanna-like woodland mosaic, this typology balanced evolutionary prospect and refuge. Scattered tree clusters created a partial enclosure, with water bodies interlaced between the woodland edges, retaining clear navigable sightlines while affording modest psychological shelter (Fig. 2b)[4]. (3) Closed Blue-Green Space (BG-C, canopy cover 90%): Simulating a dense urban riparian forest, this configuration featured multi-layered, overlapping vegetation canopies enveloping tranquil water surfaces. This vertical structural density severely restricted distant visual penetration, creating a profound sense of spatial enclosure and psychological privacy (Fig. 2c)[3, 14]. (4) Open Green Space (G-O, canopy cover 10%): An expansive grassland environment completely devoid of blue space elements. With minimal vertical obstruction from sparsely distributed solitary trees and low shrubs, it allowed participants to perform near-panoramic visual exploration, analogous to a spacious urban park meadow or open recreational field (Fig. 2d)[15]. (5) Semi-Open Green Space (G-SO, canopy cover 50%): This scenario simulated a

typical urban woodland-grassland ecotone. Strategically placed vegetation clusters defined the spatial boundaries, providing structural rhythm and shade while maintaining linear visual continuity along the standardized park pathways (Fig. 2e)[16]. (6) Closed Green Space (G-C, canopy cover 90%): Designed as a dense urban shelterbelt, the compact vertical and horizontal structure of the vegetation completely obstructed distant views. This created a secluded “urban forest” microhabitat, offering absolute visual isolation from the broader park context (Fig. 2f)[17]. (7) Urban Grey Space (UG): Serving as the nature-deprived control, this scenario was constructed as a high-rise urban canyon featuring modern architectural forms and hard-paved surfaces. To maintain equivalent navigable affordances across all conditions, building interiors were inaccessible, restricting spatial exploration strictly to the open, hard-scaped street corridors (Fig. 2g)[18].

All scenarios were modeled in SketchUp 2025 Pro and rendered in Twinmotion 2025.2. Native species, including Sophora japonica and Fraxinus chinensis, were standardized for height and crown spread. To purify the experimental variable of spatial structure, we enforced a chromatic exclusion protocol: all vegetation was rendered in a peak-summer green phenology, with flowering and chromatic foliage strictly excluded. Global illumination was provided by a unified High Dynamic Range Imaging (HDRI) directional light system (simulating 14:00 clear-sky conditions), ensuring identical solar angles and skybox backgrounds. Automatic exposure was disabled in favor of a Fixed Exposure Value (EV) with a standardized white balance of 6500K. Mean scene luminance values were verified via in-engine photometric readings to ensure that perceived brightness differences were attributable to spatial structural variation rather than lighting inconsistencies. Dynamic elements (flowing water and wind-animated foliage) were implemented via particle systems, while ambient audio was omitted to isolate visual influences on physiological restoration.

2.2.3 Locomotion and navigable affordances

To ensure comparable exposure opportunity, all scenarios included the same standardized navigable pathways, and virtual locomotion speed was capped at 1 m/s to approximate recreational walking pace[6]. During the recovery phase, participants explored the assigned environment along a predefined route structure, thereby standardizing overall navigability while preserving local visual experience.

2.3 Participants, ethics and sample size rationale

2.3.1 Participants

A total of 170 healthy young adults were recruited via public advertisement. All reported normal or corrected vision and no history of neurological or psychiatric disorders. Following protocol completion, Simulator Sickness Questionnaire (SSQ) scores were screened to ensure VR tolerance[19]. Thirteen participants exceeding the predefined motion-sickness threshold were excluded, yielding a final sample of 157 individuals (115 females, 41 males, 1 other; 91.1% aged 18–25 years). All participants had completed or were undergoing higher education.

2.3.2 Sample size rationale

Because no prior study had reported directly comparable effect sizes for a seven-condition immersive VR design integrating subjective, autonomic, endocrine, immune, and fNIRS endpoints, a formal a priori power calculation based on a single outcome would have been poorly constrained. We therefore adopted a design-based target of approximately 20–25 participants per condition, which is consistent with mechanistic laboratory studies using similarly intensive physiological protocols and was judged sufficient to estimate moderate condition effects while maintaining feasible biosignal acquisition quality. This yielded a planned sample of approximately 160–170 participants, with the final analyzed sample closely matching that target. The study should therefore be interpreted as a multimodal mechanistic experiment optimized for controlled inference rather than a single-endpoint clinical trial.

2.3.3 Physiological standardization and ethics

To reduce diurnal variation in endocrine markers, particularly salivary cortisol, all sessions were conducted between 13:00 and 18:00[20]. Participants were instructed to refrain from food, caffeine, alcohol, and nicotine for at least 2 h and from strenuous exercise for 24 h before testing. Female participants self-reported menstrual cycle phase and oral contraceptive use; when feasible, scheduling was aligned with the follicular phase to reduce HPA-axis variability. The study protocol was approved by the Institutional Review Board of Northwest A&F University and complied with the Declaration of Helsinki. Written informed consent was obtained from all participants prior to testing, and monetary compensation was provided.

2.4 Randomization and experimental procedure

Participants were randomly assigned, in an approximately balanced between-subject design, to one of the seven recovery environments. To minimize carryover and expectancy effects, each participant completed only one recovery condition. The experimental protocol lasted approximately 60 min and consisted of five consecutive phases (Fig. 3).

(1) Phase 1: Baseline (T1, 0–15 min)

Participants underwent a 10-minute seated adaptation period with the VR HMD operating in passthrough (mixed-reality) mode to maintain visual neutrality. Baseline salivary samples (S1) and pre-test psychological inventories (STAI, PANAS) were then collected. The phase concluded with a 1-minute continuous resting-state physiological recording while participants faced a blank wall in passthrough mode, establishing the baseline.

(2) Phase 2: Acute stress induction (T2, 15–20 min)

Acute psychophysiological stress was induced using a 5-minute adaptive mental arithmetic task, functioning as the core cognitive stressor of the virtual reality Trier Social Stress Test (VR-TSST)[21]. Participants remained in the VR passthrough mode facing a blank wall to eliminate environmental visual confounders. Continuous fNIRS and autonomic tracking were maintained to capture peak stress reactivity.

(3) Phase 3: Buffer period (T3, 20–28 min)

An 8-minute buffer phase immediately followed the stressor to accommodate the physiological latency of HPA axis activation and capture the delayed salivary cortisol peak[22]. Continuous fNIRS and autonomic tracking were maintained. Participants completed mid-test stress appraisals, after which the second salivary sample (S2, representing post-stress peak arousal) was collected. Participants then rested with their eyes closed while the VR simulation seamlessly transitioned to the starting point of the designated spatial landscape.

(4) Phase 4: Landscape immersion and recovery (T4, 28–58 min; Analytical Recovery Window: 0–30 min)

Participants were randomly assigned to one of the seven landscape scenarios (between-subjects design) for a 30-minute immersive recovery phase. They navigated through the virtual environment along a standardized trajectory. This 30-minute landscape immersion (T4: 28–58 min post-baseline) was statistically operationalized as the continuous recovery window (0–30 min) for spatiotemporal GAMM and fNIRS time-series modeling, with t = 0 strictly defined as the exact moment of virtual landscape onset. Continuous fNIRS and autonomic tracking were maintained to map the kinetics of cortical and autonomic restoration throughout this exposure.

(5) Phase 5: Post-immersion assessment (58–60 min)

Immediately upon concluding the 30-minute immersion, the final salivary sample (S3, representing post-recovery homeostasis) was collected. Post-test psychological evaluations and the SSQ were administered before equipment detachment, concluding the protocol.

2.5 Multimodal data acquisition

2.5.1 Psychological measures

Standardized self-report scales assessed psychological states across the experimental phases. State anxiety was evaluated using the 20-item State-Trait Anxiety Inventory (STAI-S)[23] to quantify the anxiety peak induced by the VR-TSST and subsequent recovery. Variations in affective valence were measured using the Positive and Negative Affect Schedule (PANAS), comprising Positive Affect (PANAS-PA, environmental activation) and Negative Affect (PANAS-NA, subjective distress) dimensions[24]. For consistent directionality in statistical modeling, PANAS-NA scores were reverse-coded. The Simulator Sickness Questionnaire (SSQ) was employed post-experiment solely as an exclusion criterion to filter participants with severe cybersickness, minimizing physiological confounding.

2.5.2 Peripheral autonomic monitoring

Autonomic fluctuations were tracked using a research-grade wearable device (Ruiluowei S2) recording photoplethysmography (PPG) and electrodermal activity (EDA). Data acquisition and event marking were

time-stamp synchronized via the BiovitalLab platform. The root mean square of successive differences (RMSSD) was derived from PPG inter-beat intervals (IBIs)[25]. Non-physiological IBIs (< 0.25 s or > 2.5 s) were excluded, followed by motion artifact detection using the median absolute deviation (MAD; threshold = 5)[26]. Identified artifacts were reconstructed via linear interpolation, and RMSSD was aggregated into 30-second non-overlapping epochs. For EDA, a Hampel filter (window size = 8) with 5-MAD threshold smoothed motion artifacts. A fourth-order zero-phase Butterworth filter was applied sequentially: a low-pass filter (< 0.1 Hz) extracted the skin conductance level (SCL) [27]. Finally, both continuous RMSSD and SCL data were aggregated into 30-second non-overlapping epochs[28]. SCL data were averaged over 30-second windows. Preprocessing was executed using customized scripts in R (version 4.5.2) incorporating the signal, zoo, and tidyverse packages.

2.5.3 Endocrine and immune biomarkers

Unstimulated saliva samples quantified molecular perturbations. Saliva was collected using Salivette collection tubes (Sarstedt, Nümbrecht, Germany). Participants gently chewed the provided synthetic swab for approximately 1–2 minutes to ensure adequate fluid absorption. Immediately following collection, the tubes were centrifuged at 2200g for 15 minutes at 4°C to precipitate mucins and separate the clear salivary supernatant. The extracted supernatant was then promptly aliquoted and stored at −80°C to prevent protein degradation prior to biochemical analysis. Biomarkers were assayed using Enzyme-Linked Immunosorbent Assay (ELISA) kits (ZCIBIO Technology, China). Salivary cortisol was determined via a competitive ELISA (Cat. No. ZC-54504-J); sIgA (ZC-32971), sAA (ZC-54188), and IL-6 (ZC-32446) were quantified using standard protocols[29, 30]. Samples were analyzed in duplicate wells by blinded technicians. Intra- and inter-assay coefficients of variation (CVs) were maintained below 10% and 15%, respectively.

2.5.4 Prefrontal fNIRS

Cortical hemodynamics were monitored using a continuous-wave, multi-channel fNIRS system (NirSmartII-3000A, Danyang Huichuang Medical Equipment) utilizing dual-wavelength LED sources (730 nm and 850 nm). Data were acquired at a sampling rate of 11 Hz. The probe array targeting the prefrontal and inferior frontal cortices consisted of 4 sources and 5 detectors, maintaining a standardized inter-optode distance of 30 mm to ensure optimal photon penetration into the superficial cortex. The optodes were positioned according to the international 10–20 system, with the reference probe anchored at Fpz. Following the 10–20 system spatial registration, specific channels were aggregated to define our regions of interest (ROIs): the dorsolateral prefrontal cortex (DLPFC; Brodmann Areas 9/46) and the inferior frontal gyrus pars triangularis (IFGtri; BA45)[31], which collectively constitute the core nodes of the Executive Control Network (ECN). To compute this composite ECN metric, we calculated the spatial average (mean) of the continuous oxygenated hemoglobin (HbO) concentration changes across all valid channels strictly mapped within these specific anatomical boundaries for each participant. Data were preprocessed in NirSpark. After truncating extraneous segments, a spline interpolation algorithm (moving standard deviation threshold = 6.0; amplitude threshold = 0.5) corrected

head motion artifacts. A band-pass filter (0.01–0.1 Hz) eliminated physiological and instrumental noise. Relative concentration changes in oxygenated (HbO) and deoxygenated hemoglobin (HbR) were calculated via the modified Beer-Lambert law. The differential pathlength factor (DPF) was fixed at 6.0[32]. Given its superior signal-to-noise ratio, HbO was selected as the primary hemodynamic metric. To ensure multimodal temporal alignment, continuous HbO signals were identically aggregated into 30-second non-overlapping epochs, a standardized temporal resolution optimally balancing signal stability with the fine-grained data density required for subsequent continuous trajectory modeling.

2.6 Data processing and statistical analysis

All statistical analyses and data visualizations were performed using R software (version 4.5.2). The threshold for statistical significance was set at α = 0.05 (two-tailed, unless otherwise specified for directional hypotheses). Prior to inferential testing, data distributions were assessed for normality; highly skewed neuroendocrine (salivary cortisol, sAA, IL-6, sIgA) and autonomic parameters (RMSSD) were natural-log-transformed (ln) to satisfy parametric assumptions. Due to signal quality filtering, the final analytical sample sizes for continuous physiological recordings were slightly reduced (SCL: n = 126; RMSSD: n = 135) compared to the full cohort (N = 157).

To validate stress induction and assess endpoint restorative divergence, linear mixed-effects models (LMMs; lme4, lmerTest)[33]were fitted with subject as a random intercept. Random slopes for Phase did not improve model fit and were excluded for parsimony. Stress validation was tested using Value ~ Phase + (1|Subject). Landscape-dependent recovery effects were evaluated using interaction models (Value ~ Phase × Landscape + (1|Subject)), and fine-grained typological effects were examined using three-way interactions (Value ~ Phase × SpaceType × Openness + (1|Subject)). Degrees of freedom were estimated via Satterthwaite approximation. Post-hoc contrasts were computed using emmeans with Tukey adjustment. While post-hoc pairwise contrasts were adjusted using Tukey's method within each LMM, we additionally implemented a Benjamini-Hochberg False Discovery Rate (FDR) correction across the primary interaction terms of all biological and psychological outcomes to rigorously control for Type I error inflation. All interactive and main effects reported as statistically significant successfully survived this study-wide FDR threshold ($q < 0.05$), confirming the robustness of the findings against multiple testing.

Continuous autonomic recovery dynamics were modeled using generalized additive mixed models (GAMMs; mgcv)[34], specified as SCL ~ Landscape + s (RecTime, by = Landscape, k = 12) + s (SubjectID, bs = "re"). Subject-level random effects were incorporated using penalized regression splines. To quantify recovery capacity, T_{80} (rapid autonomic recovery time) and T_{95} (near-saturated autonomic recovery time) were defined as the time required for the fitted trajectory to reach 80% and 95% of the maximal modeled recovery amplitude relative to each individual's stress peak, respectively. Net restorative load was quantified as the 30-min area under the curve (AUC). Given non-normality of SCL AUC, main environmental effects were assessed using Kruskal–Wallis tests, and factorial interactions (SpaceType × Openness) were evaluated via aligned rank transform ANOVA (ARTool)[35].

Parasympathetic dynamics (RMSSD) met parametric assumptions and were analyzed using linear models, extracting both the early 5-min slope (initial vagal rebound velocity) and total recovery AUC.

Cortical homeostatic regulation of the Executive Control Network (ECN; composite HbO across DLPFC and IFGtri) was evaluated under the Law of Initial Value (LIV)[36]. Linear regression modeled the relationship between peak stress activation and final sustained recovery level[37]. A one-tailed hypothesis test assessed whether the regression slope significantly deviated from unity ($\beta = 1$), consistent with homeostatic dampening rather than null association. To further characterize these baseline-dependent bidirectional trajectories, participants were stratified into “High ECN Activation” and “Low ECN Activation” subgroups based on their peak cortical reactivity during stress induction (T2) using a median split. This specific stratification allowed for the statistical and visual evaluation of how divergent initial cortical states convergently decay toward a uniform homeostatic baseline.

To characterize systemic psychoneuroimmunological reorganization, Gaussian graphical models (qgraph, bootnet)[38] were estimated separately for stress (T2) and recovery (T4) phases using EBICglasso regularization ($\gamma = 0.5$). Network structure and global strength invariance were tested via permutation-based Network Comparison Tests (1,000 iterations). Modularity (Q) quantified functional segregation, and participation coefficients indexed ECN integration. Stability was evaluated via case-drop bootstrapping, ensuring centrality stability coefficients exceeded 0.25[39]. Individual decoupling magnitudes (ΔCI) were subsequently compared across environmental conditions.

Finally, causal mediation analysis (mediation package[40]tested whether peripheral decoupling mediated the association between nature exposure and anxiety reduction (ΔSTAI), under the assumption of sequential ignorability. Average causal mediation effects (ACME) and average direct effects (ADE) were estimated using 10,000 bootstrap resamples to obtain bias-corrected confidence intervals.

3. Results

3.1 Acute stress produces a peripheral-dominant perturbation

Comparing the pre-stress baseline (T1) to the acute stress peak (T2), the stress induction protocol produced a robust and statistically significant shift across subjective and peripheral systems, eliciting large-magnitude and directionally coherent perturbations. Crucially, this stress response was heavily peripheral-dominant, characterized by massive autonomic, endocrine, and immune fluctuations without parallel magnitude changes in the cortical executive network.

At the subjective psychological level, the induction protocol elicited marked psychological arousal. State anxiety increased markedly following stress exposure (STAI: estimate = 0.41, 95% CI [0.33, 0.48], t_{156} = 10.79, $p < 0.001$, Hedges’ $g = 1.22$; Fig. 4a), accompanied by a pronounced reduction in positive affect (PANAS-PA: estimate = -0.60, 95% CI [-0.73, -0.48], t_{156} = -9.51, $p < 0.001$, $g = -1.07$; Fig. 4g) and a

corresponding increase in negative affect, as reflected by decreased reverse-coded scores (PANAS-NA: estimate = -0.45, 95% CI [-0.59, -0.32], t_{156} = -6.59, p < 0.001, g = -0.74; Fig. 4f), validating a definitive shift toward an anxiety-dominant emotional state.

This subjective arousal was strictly mirrored by robust activations across all measured peripheral physiological systems. Autonomic responses exhibited sympathetic dominance, reflected by elevated skin conductance levels (SCL: estimate = 0.14, 95% CI [0.09, 0.19], t_{125} = 5.24, p < 0.001, g = 0.64; Fig. 4b) alongside a modest but significant parasympathetic withdrawal indexed by reduced vagal tone (lnRMSSD: estimate = -0.07, 95% CI [-0.13, -0.02], t_{134} = -2.78, p = 0.006, g = -0.34; Fig. 4h). Endocrine measures revealed concurrent massive activation of both the hypothalamic–pituitary–adrenal and sympathetic–adrenal–medullary axes, as evidenced by surges in salivary cortisol (lnCortisol: estimate = 0.24, 95% CI [0.20, 0.28], t_{156} = 11.82, p < 0.001, g = 1.33; Fig. 4c) and α-amylase (lnsAA: estimate = 0.21, 95% CI [0.17, 0.24], t_{156} = 11.15, p < 0.001, g = 1.26; Fig. 4d). Concomitantly, stress induced marked immunological modulation, characterized by profound suppression of secretory IgA (lnsIgA: estimate = -0.23, 95% CI [-0.26, -0.20], t_{156} = -15.34, p < 0.001, g = -1.73; Fig. 4i) and rapid elevation of IL-6 (lnIL-6: estimate = 0.19, 95% CI [0.16, 0.22], t_{156} = 12.81, p < 0.001, g = 1.44; Fig. 4e), consistent with acute mucosal suppression and inflammatory priming.

In stark contrast to the large and coherent perturbations observed across subjective and peripheral systems, cortical responsiveness remained negligible. No significant phase-related modulation was observed in the executive control network (ECN HbO: estimate = -0.001, 95% CI [-0.003, 0.002], t_{156} = -0.54, p = 0.592, g = -0.06; Fig. 4j). Together, these results demonstrate a robust activation of the peripheral psychoneuroimmunological stress axis, establishing a starkly divergent perturbation baseline wherein systemic physiological reactivity overwhelmingly exceeds cortical engagement. This descriptive asymmetry provides a critical systems-level context for interpreting the subsequent recovery dynamics across different landscape configurations.

3.2 Subjective recovery converges, but peripheral recovery diverges

At the recovery endpoint, subjective psychological perception and peripheral physiological systems exhibited fundamentally distinct restorative patterns. We first evaluated subjective psychological states. At the end of the 30-minute recovery phase, nature exposure elicited a clear overarching advantage, promoting significantly higher positive affect (PANAS-PA: estimate = 0.37, 95% CI [0.02, 0.73], t_{372} = 2.08, p = 0.038, Hedges' g = 0.57; Fig. 5c) and lower state anxiety (STAI: estimate = -0.22, 95% CI [-0.42, -0.02], t_{369} = -2.15, p = 0.033, g = -0.59; Fig. 5a) compared to the urban grey (UG) space, with no statistical difference for negative affect (PANAS-NA: estimate = 0.00, 95% CI [-0.31, 0.31], t_{391} = 0.03, p = 0.979, g = 0.01; Fig. 5b). However, beneath this broad nature-urban dichotomy, subjective perception exhibited a categorical nature advantage paired with structural convergence. We found that subjective recovery was insensitive to finer spatial variations within natural spaces, consistent with a categorical perception of

naturalness. No structural determinants reached significance: neither the typological contrast of aquatic features (Blue-Green vs. Green; all $p > 0.16$; Fig. 5h–j), nor the linear and quadratic gradients of spatial openness (all $p > 0.63$), nor their higher-order Typology × Openness interaction (all $p > 0.37$; Supplementary Fig. S1a–c) yielded any detectable affective benefits. At the group level, Phase × Landscape interactions were consistently small and non-significant across all three psychological measures (STAI: $F_{12, 300} = 0.98$, $p = 0.466$, $\eta^2p = 0.038$; PANAS-PA: $F_{12, 300} = 0.88$, $p = 0.572$, $\eta^2p = 0.034$; PANAS-NA: $F_{12, 300} = 0.85$, $p = 0.597$, $\eta^2p = 0.033$; Supplementary Fig. S1d-f), confirming that recovery trajectories did not differ across the seven natural spaces. Together, these results indicate that subjective recovery converges across all natural spaces once a minimal threshold of naturalness is reached, driven by a coarse-grained perception of natural elements.

In stark contrast to this convergence in subjective perception, peripheral biochemical markers maintained acute sensitivity to distinct spaces. A significant overall effect of natural versus urban spaces was observed, with nature exposure driving systemic dampening of neuroendocrine stress and inflammatory profiles (Cortisol: estimate = -0.18, 95% CI [-0.25, -0.11], $t_{465} = -4.90$, $p < 0.001$, $g = -1.08$; sAA: estimate = -0.13, 95% CI [-0.20, -0.07], $t_{465} = -3.91$, $p < 0.001$, $g = -0.87$; IL-6: estimate = -0.26, 95% CI [-0.33, -0.19], $t_{465} = -7.36$, $p < 0.001$, $g = -1.63$; sIgA: estimate = 0.31, 95% CI [0.26, 0.37], $t_{465} = 11.12$, $p < 0.001$, $g = 2.46$; Fig. 5d-g). Yet, unlike subjective measures, physiological recovery further bifurcated based on spatial structures. At the typological level, a significant main effect of landscape typology was observed (Blue-Green vs. Green). While the addition of aquatic elements did not uniformly enhance endocrine systems (Cortisol/sAA: all $p > 0.34$; Fig. 5k, 5l), it exhibited a pronounced immune-specific advantage, selectively suppressing IL-6 (estimate = -0.10, 95% CI [-0.16, -0.05], $t_{393} = -3.62$, $p < 0.001$, $g = -0.63$; Fig. 5m) and elevating sIgA (estimate = 0.05, 95% CI [0.01, 0.09], $t_{393} = 2.22$, $p = 0.027$, $g = 0.38$; Fig. 5n). Furthermore, when evaluating the structural gradient, no significant main effect of spatial openness was observed (all $p > 0.08$).

Crucially, a highly significant Phase × SpaceType × Openness interaction emerged, indicating that the physiological impact of openness was strictly contingent upon landscape typology. Significant three-way interactions were found for sAA ($F_{4, 381} = 2.67$, $p = 0.032$, $\eta^2p = 0.027$; Fig. 5p), IL-6 ($F_{4, 381} = 35.58$, $p < 0.001$, $\eta^2p = 0.272$; Fig. 5q), and sIgA ($F_{4, 381} = 10.51$, $p < 0.001$, $\eta^2p = 0.099$; Fig. 5r), whereas cortisol remained unaffected ($F_{4, 381} = 0.49$, $p = 0.741$, $\eta^2p = 0.005$; Fig. 5o).

At the group level (Fig. 5s-v), the recovery effects resolved into a clear system-specific hierarchy. Immune recovery was the most robust and broadly distributed. Relative to UG, IL-6 was significantly reduced in five of the six landscapes, with the strongest suppression observed in BG-O (estimate = -0.37, 95% CI [-0.49, -0.25], $t_{450} = -9.44$, $p < 0.001$, $g = -2.78$), BG-C (estimate = -0.36, 95% CI [-0.48, -0.24], $t_{450} = -9.14$, $p < 0.001$, $g = -2.69$), and G-C (estimate = -0.35, 95% CI [-0.46, -0.23], t450 = -8.80, $p < 0.001$, $g = -2.59$). In contrast, G-O showed no IL-6 suppression (estimate = 0.01, 95% CI [-0.11, 0.13], $t_{450} = 0.26$, $p = 1.000$, $g = 0.08$). sIgA increased significantly in all six landscapes, with consistently large effects, particularly in BG-SO (estimate = 0.36, 95% CI [0.26, 0.46], $t_{450} = 10.26$, $p < 0.001$, $g = 3.02$), BG-O

(estimate = 0.36, 95% CI [0.25, 0.46], t_{450} = 10.28, p < 0.001, g = 3.03), and G-SO (estimate = 0.36, 95% CI [0.26, 0.47], t_{450} = 10.54, p < 0.001, g = 3.07), whereas G-O produced the smallest mucosal gain (estimate = 0.15, 95% CI [0.05, 0.26], t_{450} = 4.37, p < 0.001, g = 1.29). Endocrine recovery was more selective. Cortisol decreased significantly in BG-O (estimate = -0.19, 95% CI [-0.33, -0.04], t_{450} = -3.87, p = 0.002, g = -1.14), BG-SO (estimate = -0.21, 95% CI [-0.35, -0.06], t_{450} = -4.28, p < 0.001, g = -1.26), G-O (estimate = -0.20, 95% CI [-0.34, -0.06], t_{450} = -4.11, p < 0.001, g = -1.21), and G-SO (estimate = -0.20, 95% CI [-0.34, -0.06], t_{450} = -4.16, p < 0.001, g = -1.21), but not in the two closed spaces (BG-C: p = 0.117; G-C: p = 0.051). Autonomic recovery was the most restrictive. Significant sAA reductions were observed only in BG-O (estimate = -0.17, 95% CI [-0.31, -0.04], t_{450} = -3.81, p = 0.003, g = -1.12) and G-C (estimate = -0.18, 95% CI [-0.32, -0.05], t_{450} = -3.99, p = 0.001, g = -1.18), while BG-C, BG-SO, G-O, and G-SO did not reach significance.

Taken together, these findings delineate a clear dissociation between perceptual and biological recovery systems. Subjective responses converge rapidly once a minimal level of naturalness is achieved, reflecting a coarse categorical appraisal that is largely insensitive to finer spatial configurations. In contrast, peripheral physiological systems retain high structural specificity, with recovery trajectories differentially modulated by landscape typology and openness. This divergence resolves into a hierarchical pattern: immune markers exhibit the greatest sensitivity and consistency across environments, endocrine responses show conditional improvements primarily linked to openness, and autonomic regulation remains the most constrained and context-dependent. Overall, the data indicate that while subjective restoration reflects a threshold-based perceptual process, physiological recovery operates through a graded, system-specific mechanism that encodes detailed spatial properties of the environment.

3.3 Recovery follows a sympathetic-first, vagal-lagged hierarchy

Having established the dissociation between subjective psychological convergence and biochemical divergence at the recovery endpoint, we next examined whether natural environments alter the continuous temporal kinetics (i.e., speed and trajectory) of autonomic recovery. Continuous spatiotemporal profiling revealed a clear hierarchical sequence: recovery followed a sympathetic-first, vagal-lagged pattern, in which natural environments rapidly accelerated sympathetic withdrawal, whereas parasympathetic reactivation remained temporally delayed and largely insensitive to spatial structure. To quantify these divergent dynamics, net restorative loads and temporal trajectories were systematically evaluated across theoretically derived hierarchical levels of landscape variation.

GAMM analysis of SCL revealed highly heterogeneous and structurally contingent recovery trajectories across environments (adjusted R^2 = 0.82; Fig. 6a–i). Evaluating the overarching context (Nature vs. Urban) revealed distinct macroscopic kinetics: the aggregated natural environment facilitated a faster sympathetic withdrawal (e.g., reaching T_{80} = 0 s and T_{95} = 1155 s; Fig. 6a), whereas UG severely stalled,

delaying withdrawal onset until 338 s and deferring T_{80} to 1447 s. Similarly, at the typological level (Blue-Green vs. Green), blue-green spaces exhibited faster early saturation (T_{80} = 3 s; T_{95} = 363 s) and an earlier peak (600 s) compared to pure green spaces (T_{80} = 702 s; T_{95} = 1493 s; Fig. 6b). However, these macroscopic kinetic advantages did not translate into a significant pairwise difference in net restorative loads (Nature vs. Urban SCL AUC: estimate = − 0.11, 95% CI [−0.41, 0.19], t_{124} = − 0.71, p = 0.477, g = − 0.17; Blue-Green vs. Green SCL AUC: estimate = − 0.11, 95% CI [−0.37, 0.15], t_{104} = − 0.85, p = 0.395, g = − 0.16; Fig. 6j). This absence of a global natural advantage was driven by structural modulation within the natural spaces themselves. While neither landscape typology nor spatial openness (Openness: $F_{2, 100}$ = 1.59, p = 0.208, η^2p = 0.031) significantly dictated sympathetic withdrawal magnitude, a robust Typology × Openness interaction strictly governed the temporal kinetics (SpaceType × Openness: $F_{2, 100}$ = 10.57, p < 0.001, η^2p = 0.175; Fig. 6k).

This structural interaction generated highly non-linear and spatially differentiated trajectories, which clustered into three distinct kinetic phenotypes (Fig. 6d–i). Specifically, semi-open and closed blue-green spaces (BG-SO, BG-C) facilitated the most rapid and profound sympathetic withdrawal, achieving early saturation (T_{80}) at 0 s and 186 s, respectively (Fig. 6h, 6i). BG-SO exhibited the greatest cumulative withdrawal (AUC: 0.44 ± 0.16; Fig. 6l), significantly outperforming UG in post-hoc comparisons (UG vs. BG-SO: mean rank difference = − 36.40, SE = 11.10, t_{119} = − 3.28, p = 0.023). In contrast, Closed green space (G-C) and open blue-green space (BG-O) triggered complex, multiphasic kinetics. G-C displayed a triphasic trajectory: a rapid initial recovery (T_{80} = 169 s) that stalled into a plateau at 483 s (Value = 0.50), regressed to a dip at 794 s (Value = 0.47), and ultimately achieved deep restoration (T_{95} = 1082 s; Fig. 6f). BG-O showed an inverted-U pattern, reaching T_{80} at 529 s and T_{95} at 620 s, peaking at 699 s (Value = 0.29), but suffering a severe systemic rebound thereafter (Loss = 0.28; Fig. 6g). Conversely, structurally mismatched configurations exhibited severe temporal lag. Effective sympathetic withdrawal was noticeably delayed in G-SO (Start: 194 s; T_{80}: 1091 s; T_{95}: 1404 s) and profoundly stalled in G-O (Start: 1083 s; T_{80}: NA; T_{95}: NA; Fig. 6d, 6e), closely mirroring the sluggish profile of UG (Fig. 6c). The overall seven-group Kruskal-Wallis test confirmed significant differences in SCL AUC (χ^2_6 = 20.82, p = 0.002, ε^2 = 0.167; Fig. 6l). Together, these findings demonstrate that sympathetic withdrawal is not only accelerated by natural exposure, but is highly sensitive to fine-grained spatial structure.

In contrast, evaluating RMSSD revealed a fundamentally different temporal profile. Parasympathetic reactivation was temporally constrained and functionally decoupled from immediate environmental modulation. Neither global environmental context (Nature vs. Urban, early slope: β = 0.38, 95% CI [−1.25, 2.02], t_{133} = 0.46, p = 0.645, g = 0.11; overall AUC: estimate = 6.37, 95% CI [−0.81, 13.54], t_{133} = 1.76, p = 0.082, g = 0.41; Fig. 6m), nor typological variation (Blue-Green vs. Green, early slope: β = 0.61, 95% CI [−0.65, 1.88], t_{107} = 0.96, p = 0.340, g = 0.18; overall AUC: estimate = − 1.45, 95% CI [−7.07, 4.16], t_{107} = − 0.51, p = 0.608, g = − 0.10; Fig. 6n), nor spatial gradients and their interactions (Openness: $F_{2, 107}$ = 0.35, p = 0.702; SpaceType × Openness: $F_{2, 107}$ = 0.93, p = 0.396; Fig. 6o) significantly influenced early parasympathetic rebound or cumulative parasympathetic reactivation. Across conditions, RMSSD

trajectories exhibited near-complete convergence, with no spatial configuration, including the structurally optimal BG-SO, eliciting a significantly greater parasympathetic reactivation than UG within the 30-minute window (all pairwise $p > 0.37$, $g < 0.65$; Supplementary Fig. S2a, b). Descriptively, UG even showed a persistent downward trend (early slope: − 0.32 ± 0.98 ms/min; AUC: − 5.21 ± 4.07 ms), further underscoring the absence of rapid parasympathetic recovery.

Synthesizing these findings reveals a fundamental temporal sequence in psychophysiological restoration. Natural environments first initiate recovery by rapidly suppressing sympathetic arousal (SCL), effectively delivering an “all-clear” signal, whereas comprehensive parasympathetic reactivation (RMSSD) emerges as a delayed, secondary homeostatic process that unfolds more slowly and remains temporally decoupled from short-term spatial variation.

3.4 Peripheral decoupling explains network-level recovery

Unlike peripheral autonomic and immune systems that dynamically tracked landscape variations, the ECN exhibited no detectable spatial modulation. None of the four confirmatory contrasts yielded evidence of landscape-specific differentiation in ECN HbO (Nature vs. Urban: $F_{3, 620} = 0.11$, $p = 0.954$, $\eta^2p = 0.001$, Fig. 7a; Blue-Green vs. Green: $F_{3, 524} = 0.83$, $p = 0.477$, $\eta^2p = 0.005$, Fig. 7b; Openness: $F_{6, 508} = 0.61$, $p = 0.720$, $\eta^2p = 0.007$; SpaceType × Openness: $F_{6, 508} = 0.55$, $p = 0.769$, $\eta^2p = 0.006$; Fig. 7c). These consistently negligible effect sizes indicate little detectable configuration sensitivity. Furthermore, the overall Phase × Landscape interaction remained non-significant ($F_{18, 600} = 0.56$, $p = 0.928$, $\eta^2p = 0.017$; Fig. 7d), confirming that ECN activity was statistically independent of environmental configuration.

Notably, the absence of spatial effects was accompanied by prominent intrinsic temporal dynamics. A robust Phase × ECN Activation interaction ($F_{1, 310} = 46.68$, $p < 0.001$, $\eta^2p = 0.131$) demonstrated that ECN responses were contingent upon initial physiological states. The High ECN Activation and Low ECN Activation subgroups exhibited significant baseline divergence (T1: estimate = − 0.011, 95% CI [− 0.014, − 0.008], $t_{310} = -7.42$, $p < 0.001$, $g = -1.18$), which inverted during acute stress (T2: estimate = 0.003, 95% CI [0.0004, 0.0061], $t_{310} = 2.24$, $p = 0.026$, $g = 0.36$). Following stress cessation, both trajectories converged toward a near-zero state during recovery (T4: 0.0001 vs. −0.00004 μM), irrespective of landscape context (Fig. 7e). Regression analyses revealed a shallow slope between peak stress activation and final recovery level (raw $\beta = 0.037$, 95% CI [0.004, 0.071], standardized $\beta = 0.175$, $t_{155} = 2.22$, $p = 0.028$, Cohen’s $f^2 = 0.032$), consistent with the Law of Initial Value and indicative of baseline-dependent dampening (Fig. 7f). The regression slope significantly deviated from unity ($F_{1, 155} = 3270.93$, $p < 0.001$, Cohen’s $g_z = -4.56$). These findings suggest that ECN recovery is predominantly governed by intrinsic baseline dynamics rather than environmental modulation. This reveals a distinct cortical regulatory pattern that complements the environment-driven responses observed in peripheral systems.

To characterize multisystem coordination dynamics during psychological recovery, we applied Gaussian Graphical Models (GGMs). In these models, edges represent conditional correlations between physiological indicators (i.e., association independent of other factors), with edge thickness proportional

to statistical correlation strength. Network Comparison Tests (NCT) demonstrated significant topological reorganization of the physiological network from acute stress to recovery (Structure Invariance: M = 0.338, p = 0.001), with no difference in global network strength (S = 0.029, p = 0.934). This confirms stress recovery involves redistribution of intersystem connections rather than uniform attenuation of cross-system associations. Acute stress induced a densely integrated network configuration (modularity Q = 0.302; Fig. 7g), while recovery significantly increased network modularity (Q = 0.465, permutation p = 0.008, Cohen's g_Q = 2.45; Fig. 7h), indicating enhanced functional segregation among subsystems. The ECN exhibited negligible cross-module participation (bootstrapped median participation coefficient PC = 0.000, 95% CI [0, 0.493]), whereas IL-6 and STAI scores showed robust participation across multiple network modules (participation coefficients: 0.107, 95% CI [0, 0.511] and 0.057, 95% CI [0, 0.325], respectively; Fig. 7i), serving as stable cross-module hubs. This topology reflects ECN functional segregation in the reorganized recovery network.

Landscape context selectively modulated peripheral network reorganization. ECN cross-module participation was invariant between the two landscape types (natural vs. urban; t_{155} = -0.38, p = 0.709, g = -0.13; Fig. 7j), while peripheral autonomic–immune connectivity was significantly influenced by natural versus urban environmental conditions (t_{155} = -2.81, p = 0.008, g = -1.00; Fig. 7k). Mediation analysis confirmed reduced peripheral cross-system connectivity significantly mediated anxiety alleviation (average causal mediation effect ACME = 0.172, 95% CI [0.049, 0.322], p = 0.012), accounting for a substantial 95% proportion of the total effect (Proportion Mediated = 0.946; Fig. 7l). In contrast, there was no direct landscape effect on anxiety (average direct effect ADE = 0.010, 95% CI [-0.228, 0.267], p = 0.888).

Collectively, these findings show psychological recovery is characterized by increased physiological network modularity. Landscape health-promoting effects are primarily exerted via peripheral network restructuring, rather than direct modulation of central neurocognitive systems.

4. Discussion

4.1 Subjective convergence masks peripheral divergence

The present study shows that subjective restoration and physiological restoration do not necessarily operate at the same level of environmental sensitivity[41]. After the recovery exposure, participants reported broadly similar affective benefits across natural settings relative to urban grey space, whereas peripheral biochemical markers remained sensitive to finer-grained spatial configuration. This dissociation suggests that self-reported restoration may compress heterogeneous natural environments into a relatively coarse experiential category, while peripheral systems continue to register biologically relevant differences among spatial forms. In this sense, the findings do not challenge the broader evidence that urban nature benefits mental health[1], but they do indicate that generalized naturalness

and biologically differentiated recovery are not equivalent phenomena. Environments that feel similarly restorative may still differ in the extent to which they dampen endocrine and immune stress activity[42].

This distinction was most evident in the interaction between landscape typology and openness. Water did not uniformly improve all outcomes, and openness did not function as a simple monotonic gradient. Instead, the physiological meaning of openness depended on whether it was embedded in a blue-green or pure-green setting. This pattern is consistent with the view that restorative environments are structured spatial experiences rather than undifferentiated “nature doses.” Prior work on blue space has shown that water can alter affective appraisal and perceived restorativeness beyond greenness alone[3], while prospect-refuge theory implies that openness and enclosure are evaluated in relation to safety, shelter, and visual exposure rather than as universally beneficial or adverse conditions[43]. The present results extend that logic by showing that the same structural openness can be associated with different peripheral recovery profiles depending on the wider landscape context in which it occurs[44].

4.2 Recovery follows a sympathetic-first, vagal-lagged sequence

A second contribution of this study is that recovery was not physiologically uniform, but temporally layered. Continuous autonomic modeling indicated that environmental effects emerged more clearly in sympathetic withdrawal than in vagally weighted recovery, supporting a sympathetic-first, vagal-lagged sequence. This finding is compatible with the classical proposition that natural environments can promote relatively rapid post-stress downregulation[6], but it also refines that view by showing that not all branches of the stress system respond on the same timescale[8, 45].

In our present study, SCL trajectories were clearly structured by landscape configuration, whereas RMSSD showed limited differentiation within the 30-min recovery window. This suggests that early recovery may be driven primarily by attenuation of sympathetic arousal, while parasympathetic re-engagement unfolds more slowly and may require either a longer exposure period or richer multisensory cues to become configuration-sensitive[47, 48]. Thus, the restorative consequences of landscape design are not only a matter of endpoint magnitude, but also of temporal organization. Some configurations appear to accelerate the early withdrawal of stress, whereas others may be less effective in promoting rapid autonomic settling.

4.3 Recovery is more consistent with peripheral reorganization than with direct cortical replenishment

The third and most conceptually important contribution is that the observed recovery patterns are more consistent with peripheral reorganization than with direct cortical replenishment. Across the recovery phase, the present prefrontal ECN proxy showed little evidence of landscape-specific differentiation and instead followed baseline-dependent convergence consistent with the Law of Initial Value[49–51]. By contrast, peripheral systems displayed clearer spatial sensitivity, and network analysis showed that

recovery involved increased modularity together with reduced peripheral cross-system connectivity. Moreover, the association between natural exposure and anxiety reduction was statistically mediated by peripheral decoupling. Taken together, these findings suggest that, under the present paradigm, environmental recovery may be better understood as a process in which autonomic-immune coordination is reorganized first, thereby creating conditions conducive to broader stabilization of the stress system.

Importantly, these findings should not be interpreted as a rejection of Attention Restoration Theory (ART), but instead help specify a boundary condition for it. Although ART emphasizes the replenishment of depleted attentional resources in natural environments[7], we found no detectable landscape-specific modulation in the present prefrontal ECN proxy[52, 53]. Under the conditions tested here, recovery was more consistently associated with peripheral autonomic-immune reorganization than with measurable executive cortical differentiation. This suggests that, in acute post-stress recovery, environmental effects may become evident first in the reduction of peripheral physiological disturbance and cross-system coupling, rather than in immediately observable changes in prefrontal control-related activity[54–56]. Our results therefore refine, rather than reject, existing restoration theory by indicating that the dominant detectable pathway may depend on the type of stress, the duration and modality of exposure, and the physiological system under observation.

4.4 Limitations and Future Directions

Several limitations should be acknowledged. First, the study was conducted in a relatively homogeneous sample of healthy young adults and was strongly female-skewed, which limits generalizability to older adults, more balanced community samples, and clinical populations[57, 58]. Second, Although the present study applies a hierarchical analytical framework, a formal preregistration and a fully predeclared confirmatory hierarchy were not reported. The confirmatory versus exploratory status of individual findings should therefore be interpreted cautiously, particularly for the network-level and mechanistic analyses[59, 60]. Third, the present VR paradigm was designed for mechanistic isolation rather than full ecological realism: recovery occurred in a visual-only, seated, controller-based setting that excluded ambient sound, smell, thermal variation, social interaction, and self-paced locomotion[61]. In addition, cortical inference was limited to a prefrontal ECN proxy, and the absence of detectable spatial effects in this measure does not exclude the possibility that other networks, including salience or default-mode systems, participate in environmental recovery. Finally, salivary biomarkers were sampled discretely, RMSSD was interpreted without explicit respiratory control, and mediation and network analyses should be understood as statistical rather than definitive causal evidence[48]. Future work should therefore combine preregistered designs, more diverse samples, richer multisensory exposure paradigms, longer recovery windows, and broader neural measurements to determine whether the peripheral reorganization observed here is a stable mechanism of environmental recovery or a context-specific pattern tied to acute stress and short-term exposure.

5. Conclusion

Using a full-factorial virtual-reality paradigm that integrated subjective, autonomic, endocrine, immune, and prefrontal measures, this study shows that stress recovery in urban landscape settings is not governed by naturalness alone, but also by spatial configuration. Three main conclusions emerge. First, subjective restoration converged across natural environments, whereas peripheral physiological recovery remained sensitive to differences in landscape typology and structural openness. Second, recovery followed a sympathetic-first, vagal-lagged temporal pattern, indicating that early autonomic downregulation and later vagally weighted recovery do not unfold on the same timescale. Third, the observed recovery patterns were more consistently aligned with peripheral autonomic-immune reorganization than with detectable modulation of the present prefrontal ECN proxy.

In summary, these findings support a more configuration-sensitive and multisystem view of restorative environments. Rather than suggesting that all natural settings are biologically equivalent, the results indicate that different spatial forms may produce similar subjective relief while differing in their peripheral physiological consequences. In this sense, urban landscape design may influence stress recovery not only through the presence of nature, but through the way environmental structure shapes the organization of peripheral stress-regulatory systems.

References

1. Bratman GN et al (2019) Nature and mental health: An ecosystem service perspective. Sci Adv 5:eaax0903
2. White MP et al (2019) Spending at least 120 minutes a week in nature is associated with good health and wellbeing. Sci Rep 9:7730
3. White M et al (2010) Blue space: The importance of water for preference, affect, and restorativeness ratings of natural and built scenes. J Environ Psychol 30:482–493
4. Gatersleben B, Andrews M (2013) When walking in nature is not restorative—The role of prospect and refuge. Health Place 20:91–101
5. Coburn A et al (2017) Buildings, beauty, and the brain: A neuroscience of architectural experience. J Cogn Neurosci 29:1521–1531
6. Ulrich RS et al (1991) Stress recovery during exposure to natural and urban environments. J Environ Psychol 11:201–230
7. Kaplan S (1995) The restorative benefits of nature: Toward an integrative framework. J Environ Psychol 15:169–182
8. Thayer JF et al (2009) Heart rate variability, prefrontal neural function, and cognitive performance: the neurovisceral integration perspective on self-regulation, adaptation, and health. Ann Behav Med 37:141–153
9. Slavich GM (2020) Social safety theory: a biologically based evolutionary perspective on life stress, health, and behavior. Annu Rev Clin Psychol 16:265–295

10. Dzhambov AM et al (2020) Analytical approaches to testing pathways linking greenspace to health: a scoping review of the empirical literature. Environ Res 186:109613
11. Browning MH et al (2020) Can simulated nature support mental health? Comparing short, single-doses of 360-degree nature videos in virtual reality with the outdoors. Front Psychol 10:2667
12. Yin J et al (2018) Physiological and cognitive performance of exposure to biophilic indoor environment. Build Environ 132:255–262
13. Völker S, Kistemann T (2011) The impact of blue space on human health and well-being–Salutogenetic health effects of inland surface waters: A review. Int J Hyg Environ Health 214:449–460
14. Chiang YC et al (2017) Wild or tended nature? The effects of landscape location and vegetation density on physiological and psychological responses. Landsc Urban Plan 167:72–83
15. Wang X et al (2016) Stress recovery and restorative effects of viewing different urban park scenes in Shanghai, China. Urban Urban Green 15:112–122
16. Jiang B et al (2014) A dose of nature: Tree cover, stress reduction, and gender differences. Landsc Urban Plan 132:26–36
17. Tsunetsugu Y et al (2010) Trends in research related to Shinrin-yoku (taking in the forest atmosphere or forest bathing) in Japan. Environ Health Prev Med 15:27–37
18. Browning RC et al (2006) Effects of obesity and sex on the energetic cost and preferred speed of walking. J Appl Physiol 100:390–398
19. Kennedy RS et al (1993) Simulator sickness questionnaire: An enhanced method for quantifying simulator sickness. Int J Aviat Psychol 3:203–220
20. Kudielka BM et al (2004) HPA axis responses to laboratory psychosocial stress in healthy elderly adults, younger adults, and children: impact of age and gender. Psychoneuroendocrinology 29:83–98
21. Jönsson P et al (2010) Cardiovascular and cortisol reactivity and habituation to a virtual reality version of the Trier Social Stress Test: a pilot study. Psychoneuroendocrinology 35:1397–1403
22. Dickerson SS, Kemeny ME (2004) Acute stressors and cortisol responses: a theoretical integration and synthesis of laboratory research. Psychol Bull 130:355–391
23. Spielberger CD (1983) State-Trait Anxiety Inventory for Adults. APA PsycTests
24. Watson D et al (1988) Development and validation of brief measures of positive and negative affect: the PANAS scales. J Pers Soc Psychol 54:1063–1070
25. Schäfer A, Vagedes J (2013) How accurate is pulse rate variability as an estimate of heart rate variability? A review on studies comparing photoplethysmographic technology with an electrocardiogram. Int J Cardiol 166:15–29
26. Leys C et al (2013) Detecting outliers: Do not use standard deviation around the mean, use absolute deviation around the median. J Exp Soc Psychol 49:764–766
27. Boucsein W (2012) Electrodermal Activity. Springer Science & Business Media

28. Shaffer F et al (2020) A critical review of ultra-short-term heart rate variability norms research. Front Neurosci 14:594880
29. Nater UM, Rohleder N (2009) Salivary alpha-amylase as a non-invasive biomarker for the sympathetic nervous system: current state of research. Psychoneuroendocrinology 34:486–496
30. Steptoe A et al (2007) The effects of acute psychological stress on circulating inflammatory factors in humans: a review and meta-analysis. Psychol Bull 133:909–942
31. Pinti P et al (2020) The present and future use of functional near-infrared spectroscopy (fNIRS) for cognitive neuroscience. Ann N Y Acad Sci 1464:5–29
32. Scholkmann F, Wolf M (2013) General equation for the differential pathlength factor of the frontal human head depending on wavelength and age. J Biomed Opt 18:105004
33. Bates D et al (2015) Fitting linear mixed-effects models using lme4. J Stat Softw 67:1–48
34. Wood SN (2017) Generalized Additive Models: An Introduction with R. CRC
35. Wobbrock JO et al (2011) The aligned rank transform for nonparametric factorial analyses using only anova procedures. *Proc. SIGCHI Conf. Hum. Factors Comput. Syst.* 143–146
36. Wilder J (1957) The law of initial value in neurology and psychiatry. J Nerv Ment Dis 125:73–86
37. Niendam TA et al (2012) Meta-analytic evidence for a superordinate cognitive control network subserving diverse executive function. Cogn Affect Behav Neurosci 12:241–268
38. Epskamp S, Fried E (2018) I. A tutorial on regularized partial correlation networks. Psychol Methods 23:617–634
39. Epskamp S et al (2018) Estimating psychological networks and their accuracy: A tutorial paper. Behav Res Methods 50:195–212
40. Tingley D et al (2014) mediation: R package for causal mediation analysis. J Stat Softw 59:1–38
41. Markevych I, Schoierer J, Hartig T, Chudnovsky A, Hystad P, Dzhambov AM, Fuertes E (2017) Exploring pathways linking greenspace to health: Theoretical and methodological guidance. Environ Res 158:301–317
42. Kuo M (2015) How might contact with nature promote human health? Promising mechanisms and a possible central pathway. Front Psychol 6:1093
43. Dosen AS, Ostwald MJ (2016) Evidence for prospect-refuge theory: a meta-analysis of the findings of environmental preference research. City territory Archit 3(1):4
44. Gascon M, Zijlema W, Vert C, White MP, Nieuwenhuijsen MJ (2017) Outdoor blue spaces, human health and well-being: A systematic review of quantitative studies. Int J Hyg Environ Health 220(8):1207–1221
45. Yao X et al (2024) Quantifying threshold effects of physiological health benefits in greenspace exposure. Landsc Urban Plan 241:104917
46. Jin Y et al (2024) Quantifying physiological health efficiency and benefit threshold of greenspace exposure in typical urban landscapes. Environ Pollut 362:124726
47. Porges SW (2007) The polyvagal perspective. Biol Psychol 74:116–143

48. Laborde S, Mosley E, Thayer JF (2017) Heart rate variability and cardiac vagal tone in psychophysiological research - recommendations for experiment planning, data analysis, and data reporting. Front Psychol 8:213
49. Bratman GN et al (2015) Nature experience reduces rumination and subgenual prefrontal cortex activation. *Proc. Natl. Acad. Sci. U.S.A.* 112, 8567–8572
50. Sudimac S, Sale V, Kühn S (2022) How nature nurtures: Amygdala activity decreases as the result of a one-hour walk in nature. Mol Psychiatry 27:4446–4452
51. Wilder J (1962) Basimetric approach (law of initial value) to biological rhythms. Ann N Y Acad Sci 98:1211–1220
52. Craig AD (2002) How do you feel? Interoception: the sense of the physiological condition of the body. Nat Rev Neurosci 3:655–666
53. McEwen BS (1998) Protective and damaging effects of stress mediators. N Engl J Med 338:171–179
54. Sterling P, Eyer J (1988) Allostasis: a new paradigm to explain arousal pathology. In *Handbook of Life Stress, Cognition and Health* (eds Fisher, S. & Reason, J.) 629–649 (John Wiley & Sons
55. Seeley WW et al (2007) Dissociable intrinsic connectivity networks for salience processing and executive control. J Neurosci 27:2349–2356
56. Friston K (2010) The free-energy principle: a unified brain theory? Nat Rev Neurosci 11:127–138
57. Deng H et al (2025) Daily mobility, greenspace exposure and affective states. Landsc Urban Plan 262:105407
58. Ramanpong J et al (2025) Effects of forest bathing and the influence of exposure levels on cognitive health in the elderly. Urban Urban Green 104:128667
59. Kramer M et al (2025) Nature exposure impacts affect and brain activation in health and major depression. J Environ Psychol 106:102730
60. Song R et al (2022) Psychophysiological restorative potential in cancer patients by virtual reality (VR)-based perception of natural environment. Front Psychol 13:1003497
61. Browning MH et al (2020) An actual natural setting improves mood better than its virtual counterpart: A meta-analysis of experimental data. Front Psychol 11:2200

Figures

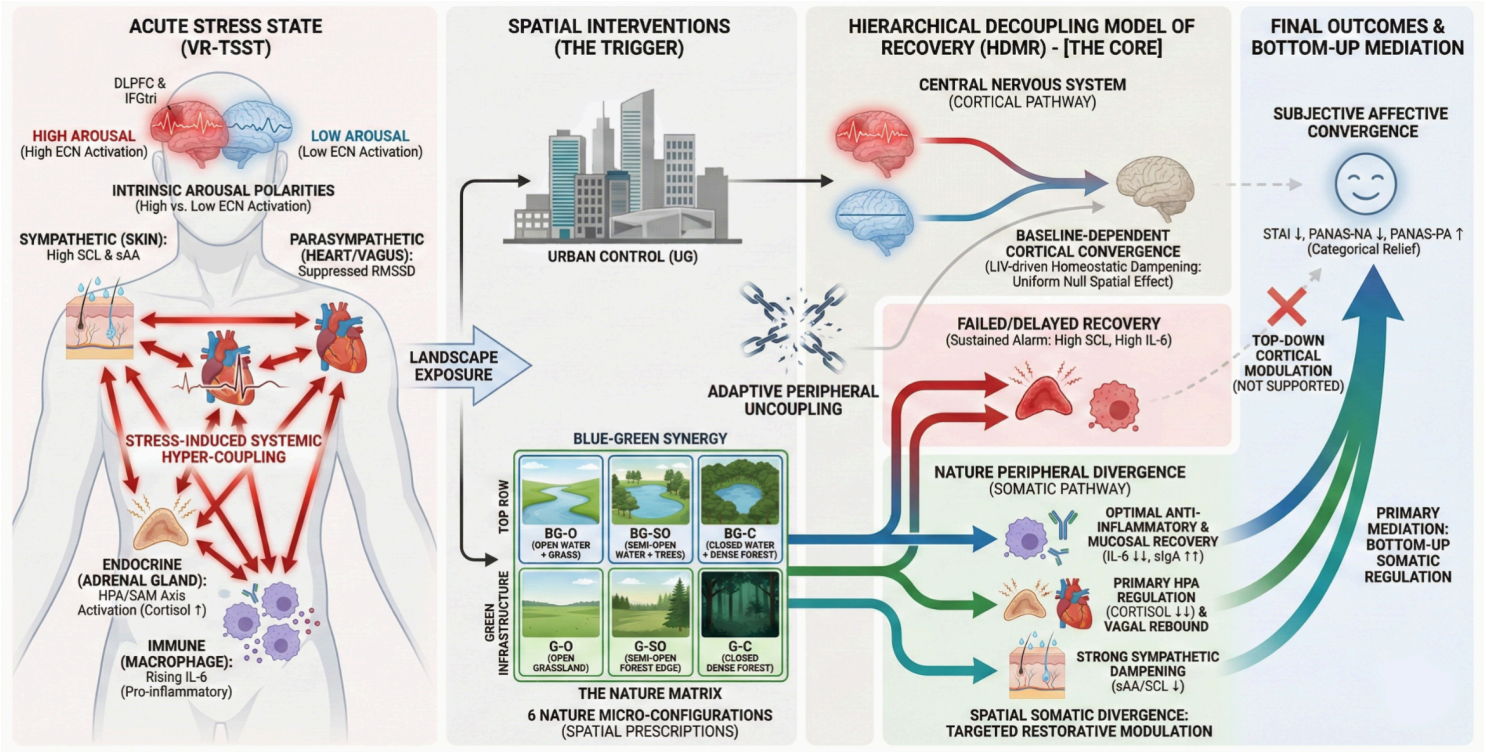


Figure 1

The Hierarchical Model of Recovery (HMR). Acute stress triggers rigid systemic hyper-coupling across central and peripheral networks. Following landscape interventions, this homeostatic network undergoes adaptive peripheral decoupling. Cortical pathways exhibit baseline-dependent convergence (governed by the Law of Initial Value), demonstrating a null spatial effect. Conversely, peripheral systems manifest spatial somatic divergence, enabling targeted restorative modulation. Ultimately, subjective affective relief is driven by bottom-up somatic regulation rather than top-down cortical pathways.



Figure 2

Experimental landscape matrix and spatial configurations. The full-factorial virtual environments (3 × 2 design plus control) isolating structural openness and blue-green composition. **a–c**, Blue-green spaces featuring standardized water bodies with canopy cover at 10% (Open, BG-O; **a**), 50% (Semi-open, BG-SO; **b**), and 90% (Closed, BG-C; **c**). **d–f**, Pure green spaces devoid of water across corresponding structural gradients: 10% (G-O; **d**), 50% (G-SO; **e**), and 90% (G-C; **f**). **g**, High-density Urban Grey Space (UG) serving as the nature-deprived baseline. Base terrains, botanical assets, and photometric parameters were strictly standardized across all scenarios to ensure absolute variable isolation.

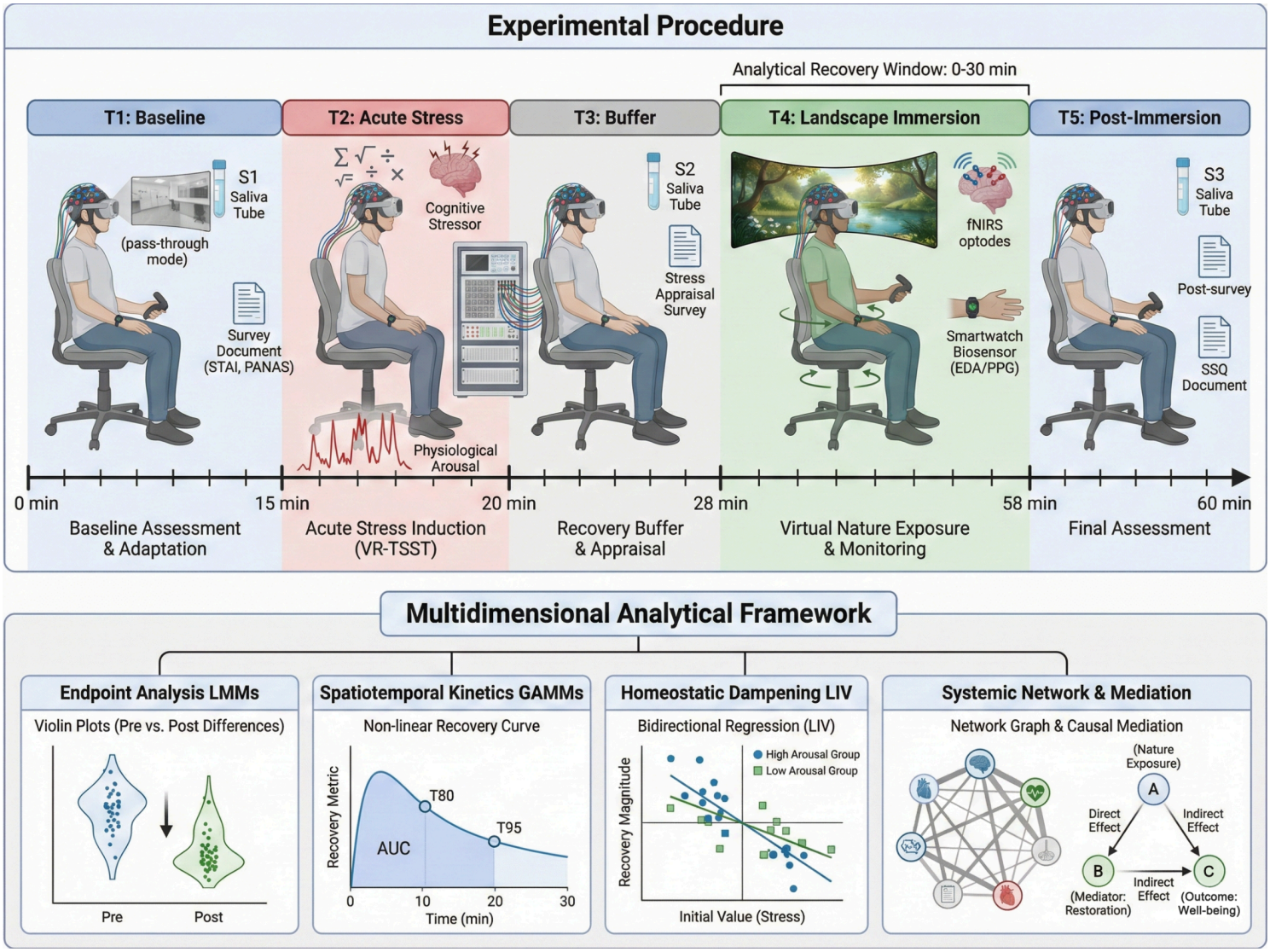


Figure 3

Experimental timeline and multimodal analytical framework for stress induction and recovery. Top: The 60-minute time-locked experimental protocol (T1–T5). Participants were continuously instrumented with a VR head-mounted display and a multi-channel fNIRS cap tethered to the data acquisition system. To strictly eliminate motion artifacts in peripheral autonomic signals, participants remained seated on an ergonomic swivel chair with their non-dominant hand (wearing the biosensor) completely motionless on their lap, while operating the VR controller with their dominant hand. During the landscape immersion (T4; statistically operationalized as the 0–30 min core analytical recovery window), spatial exploration was achieved via trunk and head rotation rather than physical ambulation. **Bottom**: The multimodal statistical and network modeling framework, comprising four independent analytical modules: (1) Endpoint static restorative divergence evaluated via Linear Mixed-Effects Models (LMMs); (2) Continuous spatiotemporal autonomic kinetics and capacity thresholds (T_{80} and T_{95}) modeled via Generalized Additive Mixed Models (GAMMs); (3) Cortical homeostatic dampening effects validated via the Law of Initial Value (LIV); and (4) Cross-system topological reorganization mapped via Gaussian Graphical Models (GGMs) alongside causal mediation analysis.

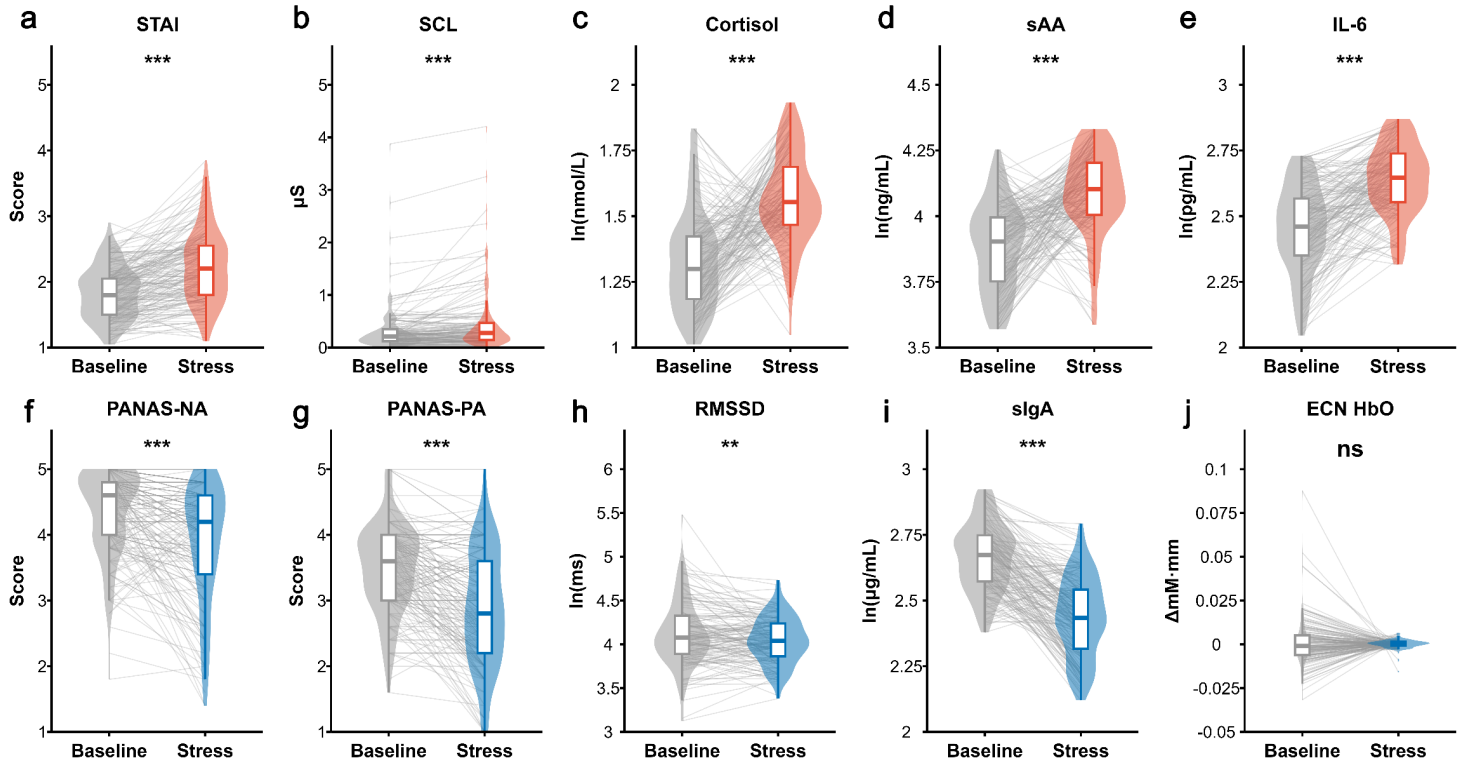


Figure 4

Acute stress produces a peripheral-dominant perturbation. a–e, Upregulated psychological and biomarker responses. Linear mixed-effects models (LMM: Value ~ Phase + (1|Subject)) pairwise comparisons between baseline and stress phases: state anxiety (**a**; t_{156} = 10.79, p < 0.001, Hedges' g = 1.22), sympathetic skin conductance level (SCL, **b**; t_{125} = 5.24, p < 0.001, g = 0.64), salivary cortisol (**c**; t_{156} = 11.82, p < 0.001, g = 1.33), alpha-amylase (sAA, **d**; t_{156} = 11.15, p < 0.001, g = 1.26), and interleukin-6 (IL-6, **e**; t_{156} = 12.81, p < 0.001, g = 1.44). **f–i**, Downregulated psychological and biomarker responses. LMM pairwise comparisons: reverse-coded negative affect (PANAS-NA, **f**; t_{156} = −6.59, p < 0.001, g = -0.74), positive affect (PANAS-PA, **g**; t_{156} = −9.51, p < 0.001, g = -1.07), vagal tone (RMSSD, **h**; t_{134} = −2.78, p = 0.006, g = -0.34), and secretory immunoglobulin A (sIgA, **i**; t_{156} = −15.34, p < 0.001, g = -1.73). **j**, ECN HbO across phases (t_{156} = −0.54, p = 0.592, g = -0.06). Highly skewed neuroendocrine and autonomic parameters were natural-log-transformed (ln) prior to analysis. Split-violin plots include boxplots (center line, median; box limits, upper and lower quartiles). Faint grey lines indicate individual within-subject trajectories across baseline and stress phases. **p < 0.01, *** p < 0.001; ns, non-significant. Valid sample sizes: overall n = 157 (SCL, n = 126; RMSSD, n = 135).

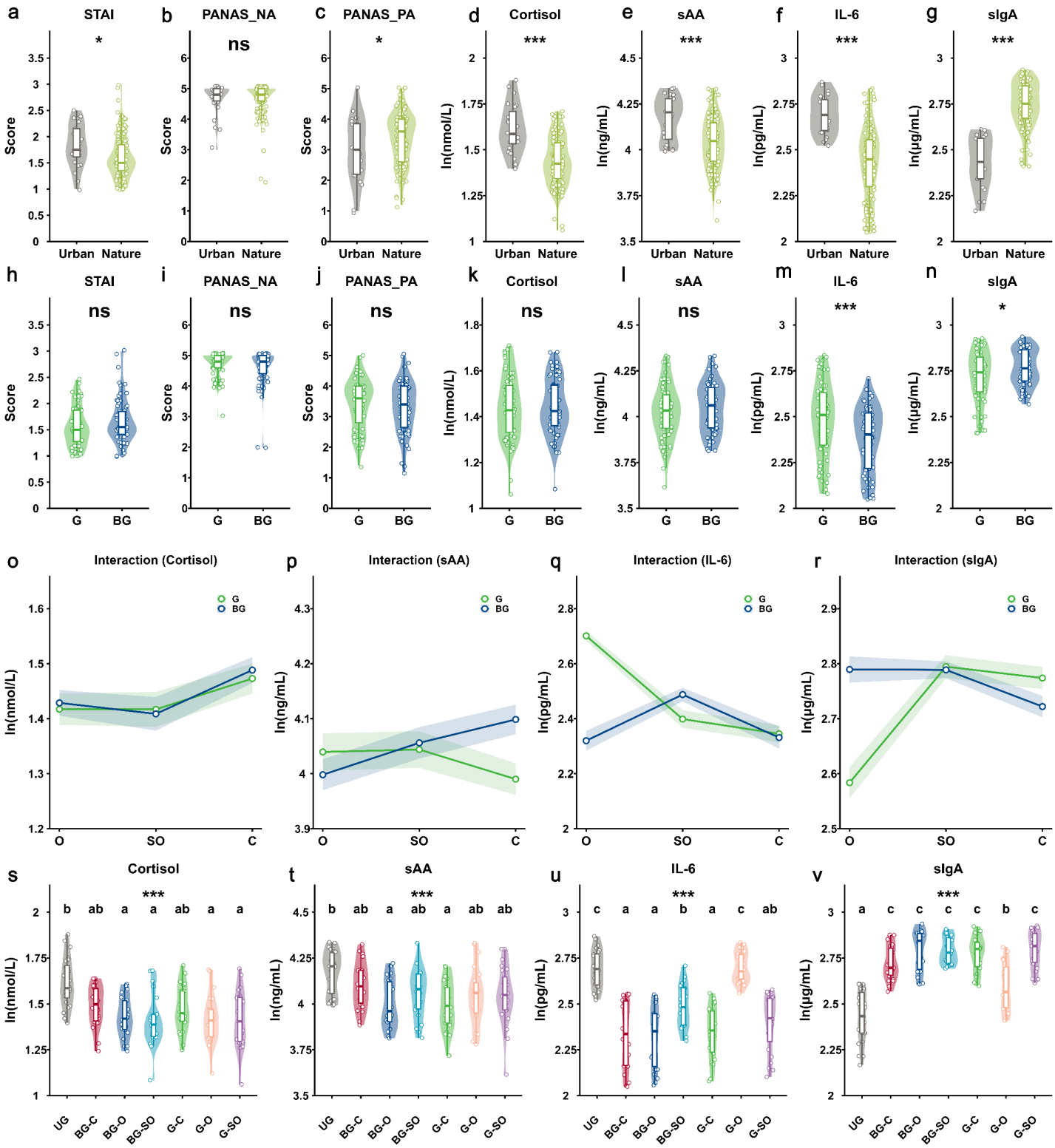


Figure 5

Subjective recovery converges, but peripheral recovery diverges. a–g, Nature vs. Urban contrasts at recovery (Recovery-phase pairwise LMM). **a**, STAI: $t_{369} = -2.15$, $p = 0.033$, $g = -0.59$. **b**, PANAS-NA: $t_{391} = 0.03$, $p = 0.979$, $g = 0.01$. **c**, PANAS-PA: $t_{372} = 2.08$, $p = 0.038$, $g = 0.57$. **d**, Cortisol: $t_{465} = -4.90$, $p < 0.001$, $g = -1.08$. **e**, sAA: $t_{465} = -3.91$, $p < 0.001$, $g = -0.87$. **f**, IL-6: $t_{465} = -7.36$, $p < 0.001$, $g = -1.63$. **g**, sIgA: $t_{465} =$

11.12, $p < 0.001$, $g = 2.46$. **h–n**, Blue-Green vs. Green contrasts at recovery. **h**, STAI: $t_{305} = 1.40$, $p = 0.161$, $g = 0.31$. **i**, PANAS-NA: $t_{312} = -0.67$, $p = 0.502$, $g = -0.15$. **j**, PANAS-PA: $t_{307} = -0.68$, $p = 0.497$, $g = -0.15$. **k**, Cortisol: $t_{393} = 0.22$, $p = 0.824$, $g = 0.04$. **l**, sAA: $t_{393} = 0.94$, $p = 0.346$, $g = 0.16$. **m**, IL-6: $t_{393} = -3.62$, $p < 0.001$, $g = -0.63$. **n**, sIgA: $t_{393} = 2.22$, $p = 0.027$, $g = 0.38$. **o–r**, Typology × Openness interactions with superimposed openness main effects (LMM: Value ~ Phase × SpaceType × Openness). **o**, Cortisol: openness $F_{2,381} = 0.77$, $p = 0.462$, $\eta^2p = 0.004$; interaction $F_{4,381} = 0.49$, $p = 0.741$, $\eta^2p = 0.005$. **p**, sAA: openness $F_{2,381} = 0.20$, $p = 0.822$, $\eta^2p = 0.001$; interaction $F_{4,381} = 2.67$, $p = 0.032$, $\eta^2p = 0.027$. **q**, IL-6: openness $F_{2,381} = 0.37$, $p = 0.694$, $\eta^2p = 0.002$; interaction $F_{4,381} = 35.58$, $p < 0.001$, $\eta^2p = 0.272$. **r**, sIgA: openness $F_{2,381} = 2.53$, $p = 0.081$, $\eta^2p = 0.013$; interaction $F_{4,381} = 10.51$, $p < 0.001$, $\eta^2p = 0.099$. **s–v**, Biochemical recovery across seven landscapes at endpoint. Significant Phase × Landscape interactions (LMM): cortisol (**s**): $F_{12,450} = 3.75$, $p < 0.001$, $\eta^2p = 0.091$; sAA (**t**): $F_{12,450} = 3.10$, $p < 0.001$, $\eta^2p = 0.076$; IL-6 (**u**): $F_{12,450} = 27.03$, $p < 0.001$, $\eta^2p = 0.419$; sIgA (**v**): $F_{12,300} = 25.31$, $p < 0.001$, $\eta^2p = 0.503$. Lowercase letters denote pairwise differences ($p < 0.05$; Tukey-adjusted LMM *post-hoc* comparisons). Highly skewed neuroendocrine parameters were natural-log-transformed (ln) prior to analysis. Violin plots include boxplots (center line, median; box limits, upper and lower quartiles) and subject-level jitter. Interaction plots display mean ± SEM. * $p < 0.05$, ** $p < 0.01$, *** $p < 0.001$; ns, non-significant (recovery-phase slice contrasts). Valid sample size: $n = 157$ (Nature, $n = 133$; Urban, $n = 24$; with $n = 22–24$ per specific spatial configuration).

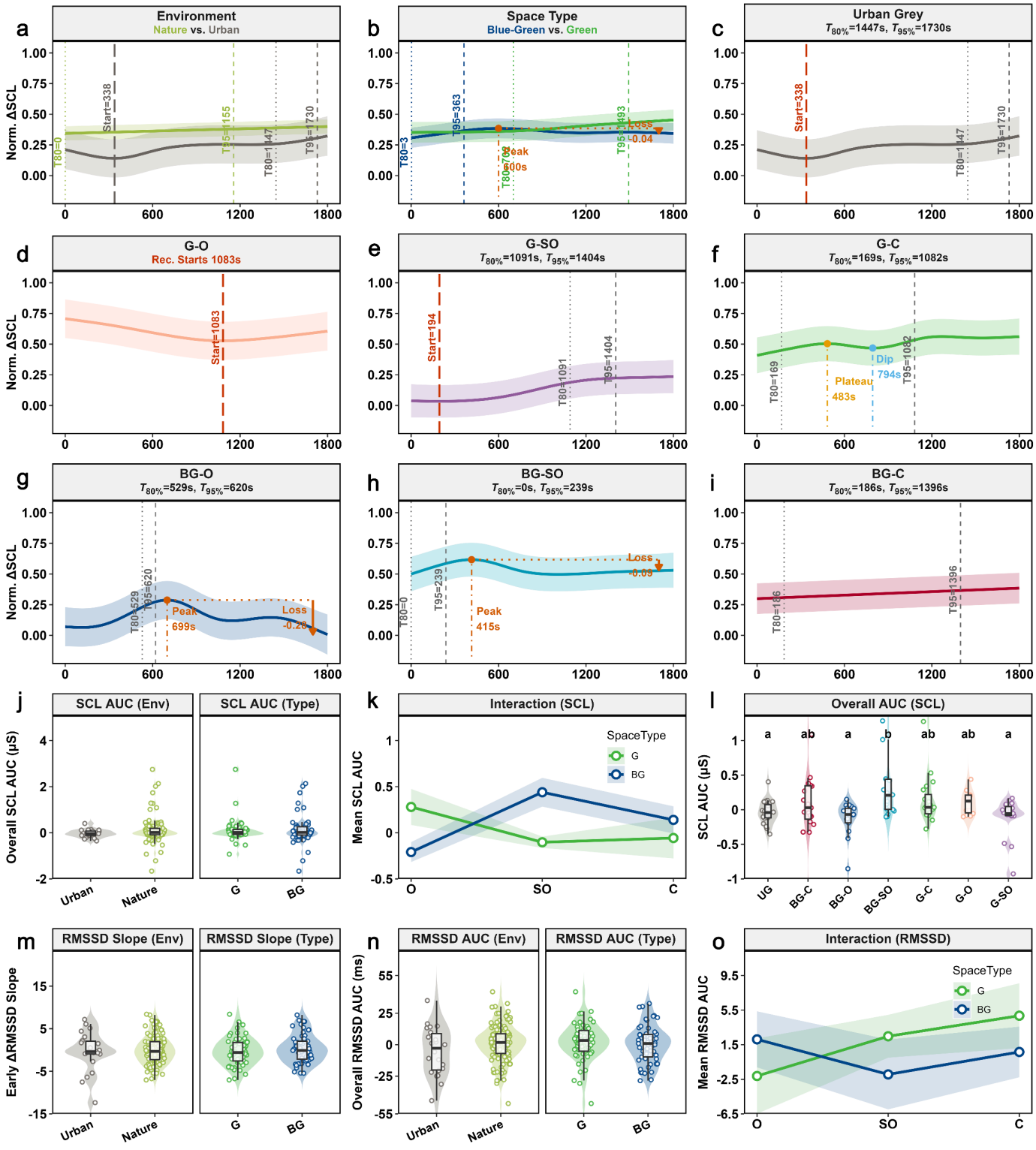


Figure 6

Recovery follows a sympathetic-first, vagal-lagged hierarchy. a–i, Continuous spatiotemporal kinetics of sympathetic withdrawal (normalized ΔSCL) analyzed via generalized additive mixed models (GAMM). Panels display aggregated trajectories for the overarching environmental context (**a**, Nature vs. Urban), spatial typologies (**b**, Blue-Green vs. Green), and seven fine-grained spatial configurations (**c–i**). Vertical lines denote 80% (T_{80}, dotted) and 95% (T_{95}, dashed) saturation thresholds; restorative onset (Start) and

peak/dip inflection points are annotated where applicable. **j**, SCL AUC across overarching and typological levels. Nature vs. Urban: estimate = −0.11 [−0.41, 0.19], t_{124} = −0.71, p = 0.477, g = −0.17; Blue-Green vs. Green: estimate = −0.11 [−0.37, 0.15], t_{104} = −0.85, p = 0.395, g = −0.16. **k**, SpaceType × Openness interaction for SCL AUC (ART ANOVA; Openness: $F_{2, 100}$ = 1.59, p = 0.208, η^2p = 0.031; SpaceType × Openness: $F_{2, 100}$ = 10.57, p < 0.001, η^2p = 0.175). **l**, SCL AUC across seven landscapes (Kruskal-Wallis: χ^2_6 = 20.82, p = 0.002, ε^2 = 0.167). **m**, Early parasympathetic velocity (first 5-min RMSSD slope) across overarching and typological levels. Nature vs. Urban: β = 0.38 [−1.25, 2.02], t_{133} = 0.46, p = 0.645, g = 0.11; Blue-Green vs. Green: β = 0.61 [−0.65, 1.88], t_{107} = 0.96, p = 0.340, g = 0.18. **n**, Cumulative parasympathetic reactivation (RMSSD AUC) across overarching and typological levels. Nature vs. Urban: estimate = 6.37 [−0.81, 13.54], t_{133} = 1.76, p = 0.082, g = 0.41; Blue-Green vs. Green: estimate = −1.45 [−7.07, 4.16], t_{107} = −0.51, p = 0.608, g = −0.10. **o**, RMSSD AUC SpaceType × Openness interaction (Openness: $F_{2, 107}$ = 0.35, p = 0.702; SpaceType × Openness: $F_{2, 107}$ = 0.93, p = 0.396). Violin plots (**j, l, m, n**) display boxplots (center line, median; box limits, upper and lower quartiles) and subject-level jitter. Interaction plots (**k, o**) display mean ± SEM. Lowercase letters (**l**) denote significant pairwise differences (p < 0.05; rank-based *post-hoc* tests with Tukey adjustment). Valid sample sizes: SCL (n = 126; UG=20, BG-C=19, BG-O=17, BG-SO=18, G-C=19, G-O=14, G-SO=19); RMSSD (n = 135; UG=22, BG-C=21, BG-O=17, BG-SO=19, G-C=20, G-O=15, G-SO=21).

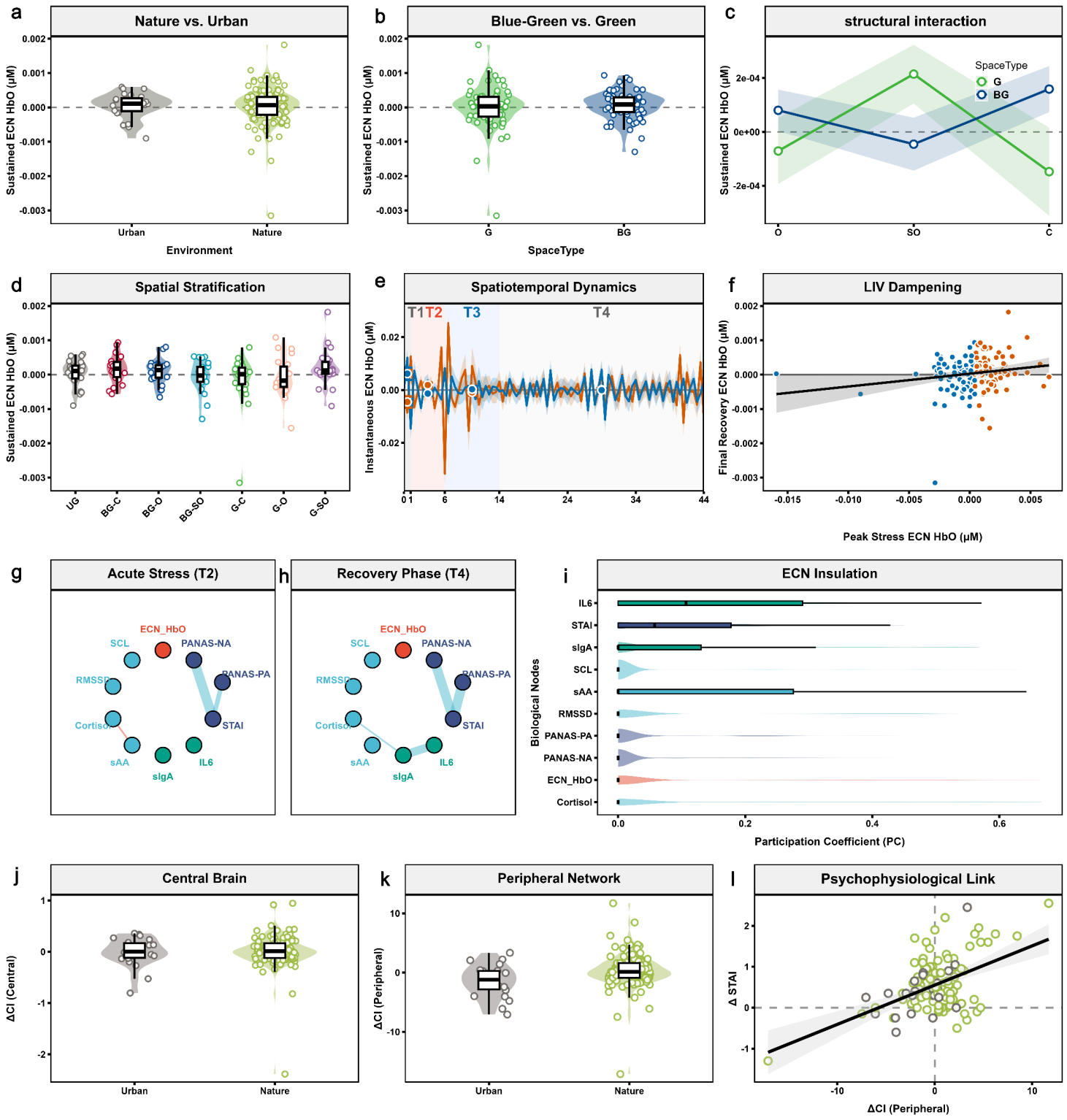


Figure 7

Peripheral decoupling explains network-level recovery. a–c, Hierarchical evaluation of sustained cortical activity (ECN HbO) during recovery, demonstrating consistent null spatial modulation across the overarching environmental context (a; Nature vs. Urban, Phase × Environment: $F_{3, 620} = 0.11$, $p = 0.954$, $\eta^2p = 0.001$), typology (b; Blue-Green vs. Green, Phase × SpaceType: $F_{3, 524} = 0.83$, $p = 0.477$, $\eta^2p = 0.005$), and structural interaction (c; Openness: $F_{6, 508} = 0.61$, $p = 0.720$, $\eta^2p = 0.007$; SpaceType × Openness: $F_{6,}$

$_{508}$ = 0.55, p = 0.769, η²p = 0.006). **d**, Overall spatial stratification across the seven independent landscapes at the recovery endpoint (Phase × Landscape interaction: $F_{18, 600}$ = 0.56, p = 0.928, η²p = 0.017). **e**, Spatiotemporal trajectories of ECN HbO across baseline (T1), stress (T2), buffer (T3), and recovery (T4) phases for High versus Low ECN Activation subgroups (bands denote mean ± SEM). LMM for Phase × Activation interaction: $F_{1, 310}$ = 46.68, p < 0.001, η²p = 0.131. **f**, Law of Initial Value (LIV) dampening effect. Linear regression of final recovery against peak stress (standardized β = 0.175, p = 0.028, Cohen's f^2 = 0.032); deviation from the no-recovery baseline ($F_{1, 155}$ = 3270.93, p < 0.001, Cohen's g_z = -4.56). **g, h**, Multisystem Gaussian Graphical Models (GGMs) during acute stress (T2; **g**) and recovery (T4; **h**). Nodes are colored by biological system; edge thickness represents partial correlation. Network Comparison Tests (NCT) for structure invariance (M = 0.338, p = 0.001) and global strength invariance (S = 0.029, p = 0.934). **i**, Bootstrapped participation coefficients (PC) at T4 indicating ECN topological insulation. Systemic modularity comparison (Q_{T2} = 0.302 vs. Q_{T4} = 0.465, permutation p = 0.008, Cohen's g_Q = 2.45). **j, k**, Central brain (**j**: t_{155} = -0.38, p = 0.709, g = -0.13) and peripheral (**k**: t_{155} = -2.81, p = 0.008, g = -1.00) decoupling magnitudes (ΔCI) across environments. **l**, Mediation of nature-induced peripheral decoupling on subjective anxiety relief (average causal mediated effect [ACME] = 0.172 [95% CI: 0.049, 0.322], p = 0.012, proportion mediated = 0.946; average direct effect [ADE] = 0.010 [95% CI: -0.228, 0.267], p = 0.888). Violin plots (**a–d, j–k**) include boxplots (center line, median; box limits, upper and lower quartiles) with subject-level jitter. Valid sample sizes vary by modality (n = 126-157).

Supplementary Files

This is a list of supplementary files associated with this preprint. Click to download.

- floatimage8.png
- floatimage9.png